Crystal structure, phase stability, and electronic structure of Ti-Al intermetallics: Ti_3Al

T. Hong, T. J. Watson-Yang,* X.-Q. Guo,† A. J. Freeman, and T. Oguchi‡
Department of Physics and Astronomy, Northwestern University, Evanston, Illinois 60208-3112

Jian-hua Xu
Shanghai Institute of Metallurgy, Academia Sinica, Shanghai 200 050, China
and Department of Physics and Astronomy, Northwestern University, Evanston, Illinois 60208-3112
(Received 8 March 1990)

A potentially useful high-temperature intermetallic compound Ti_3Al is investigated theoretically by the self-consistent linear muffin-tin orbitals (LMTO) and full-potential linearized augmented-plane-wave (FLAPW) methods within the local-density approximation. Structural properties were calculated for the naturally observed structure, $D0_{19}$, and for two other similar structures, $D0_{22}$ and $L1_2$. The LMTO-calculated Wigner-Seitz radii are 2.98 a.u. for all three structures, in excellent agreement with the experimental value (2.99 a.u.) of the observed $D0_{19}$ structure, while the values from the FLAPW method are 2.94 a.u. for the three structures, showing an agreement within about 2%. The calculated formation energies are 0.29, 0.27, and 0.29 eV/atom by the LMTO, and 0.28, 0.25, and 0.27 eV/atom by the FLAPW for the $D0_{19}$, $D0_{22}$, and $L1_2$ structures, respectively. The calculated bulk moduli are 1.2 Mbar for all the phases done by the LMTO and FLAPW except the $D0_{19}$ phase from the LMTO calculations, where the value is 1.3 Mbar. These calculated formation energies and bulk moduli agree well (to 10%) with experimental data. The FLAPW-calculated c/a ratio for the $D0_{19}$ and $D0_{22}$ structures are 0.807 and 2.131, respectively. The value for the $D0_{19}$ structure is within 1% of the observed value (0.8007) and the value for the $D0_{22}$ structure is significantly lower than the observed value (2.234) for $TiAl_3$. Charge-density plots for $D0_{19}$ and $L1_2$ show quite localized charge distributions in both phases. The covalent character of the bonding is not significant, which may be a good sign for ways to improve its poor ductility.

I. INTRODUCTION

The intermetallic compound Ti_3Al has been the subject of considerable attention by experimentalists for some years.[1–4] It is considered a desirable candidate for application in aircraft turbine engines because its static strength and stiffness do not degrade rapidly as temperatures increase and it also shows improved oxidation resistance over the conventional Ti alloys. As is the case with some other intermetallic compounds, however, Ti_3Al shows limited ductility below[3] 600–900 °C.

Ti_3Al is naturally observed in the $D0_{19}$ structure with lattice parameters[5] $a=5.77$ Å and $c/a=0.8007$. Lipsitt, Shechtman, and Schafrik[3] studied the deformation and fracture of Ti_3Al and found that the major deformation mode is the planar $\frac{1}{2}a'\langle 1120\rangle$ on $\{1010\}$, $\{0001\}$, $\{1011\}$ planes. The incidence of $c+a$ or $\langle 1123\rangle$ dislocations is very low at temperatures below 600 °C (and even at 900 °C). No twinning is observed. Intergranular cracking begins above 600 °C and increases with increasing temperature, giving rise to an apparent ductile-brittle transition. Some cross slipping also occurs above 600 °C. Both Williams and Blackburn[1] and Thomas, Vassel, and Veyssiere[4] found a predominance of α-type dislocations with a $\frac{1}{3}\langle 11\bar{2}0\rangle$ Burgers vector. From these results, we can see why it is thought that there are two ways to improve the ductility at lower temperatures: one is to stabilize the cubic $L1_2$ structure so that the dislocations with B vectors having a c component appear (simply from symmetry considerations, the c axis is equivalent to the a and b axis in the $L1_2$ structure), thereby providing enough slip systems to fulfill the requirement for ductility. Another way is to modify the fine structure through proper technological control while keeping the crystal structure. Our investigation is based on exploring the first possibility.

II. METHOD

We used the linear muffin-tin orbitals (LMTO) method[6] with the combined correction terms included, and the full-potential linearized augmented-plane-wave (FLAPW) method[7] based on the local-density functional (LDF) theory. The details of the calculations are quite similar to our previous calculations for aluminum intermetallics.[8–11] For the LMTO part, we used spherical-harmonic components up to $l=2$ in constructing basis functions, as both Ti and Al are light metals. The same size of the Wigner-Seitz sphere radius was chosen for Ti and Al. The calculations were performed with up to 210 **k** points in the irreducible Brillouin zone; an extrapolation to the case of infinite **k** points was made by using the $N_k^{-2/3}$ relation.[7] As the experimentally observed $D0_{19}$ structure is basically hexagonal close packed and the $L1_2$ and $D0_{22}$ are the corresponding cubic-based close-packed simple structures, we confined our calculations to these three structures (a geometric illustration of these three

structures is given in Fig. 1 of Ref. 8). For simplicity, we kept the c/a ratio fixed at the experimental value (0.8007) for the $D0_{19}$ lattice and at the unrelaxed value (2.0) for the $D0_{22}$ lattice.

For the FLAPW calculations, however, we performed calculations at a number of c/a ratio values and the equilibrium c/a ratios were then determined from the calculations. The l expansion for the wave function, charge density, and potential was truncated at $l=10$. More than 50 basis functions per atom were used to construct the Hamiltonian and more than 2600 plane waves per formula unit were included to represent the charge density and potential in the interstitial region. The muffin-tin radii for both Ti and Al atoms were kept the same (2.60 a.u.). The number of **k** points in the irreducible wedge of the first Brillouin zone was increased to 210 and the $N_k^{-2/3}$ relation was used again to extrapolate the results to the case of infinite number of **k** points. In all structures considered, all the necessary parameters were adjusted so that the convergence of the total energy reached 0.1 mRy.

III. RESULTS

A. LMTO calculations

The calculated structural and cohesive properties are given in Table I. We see that the calculated equilibrium lattice constants (in terms of the Wigner-Seitz radius), 2.98 a.u. for all three structures, show excellent consistency for the atomic volume of these different structures. Comparing this value with the corresponding experimental value (2.99 a.u.) (Ref. 5) for the $D0_{19}$ structure shows the agreement to be better than 0.4%. This good agreement again suggests[8–10,12,13] that the LMTO method is quite reliable for predicting the lattice constants of the close-packed structures.

The formation energies were calculated to be 0.29, 0.27, and 0.29 eV/atom for the $D0_{19}$, $D0_{22}$, and $L1_2$ structures, respectively. Surprisingly, the total-energy difference between the three structures is very small, with the values for the $D0_{19}$ and $L1_2$ structures even being the same in this approach. This may be a good indication that the cubic $L1_2$ structure might be rather easily stabilized to provide better ductility. Since the experimental heats of formation for the $D0_{19}$ structure are 0.26,[14] 0.29,[15] and 0.27 eV/atom,[16] the agreement between experimental and computational values is quite good ($<10\%$).

The bulk moduli obtained by a parabolic fit to the calculated total energy versus lattice constant are 1.3, 1.2, and 1.2 Mbar for the $D0_{19}$, $D0_{22}$, and $L1_2$ structures, respectively. These values are fairly close to the value 1.2 Mbar calculated from $B=E/[3(1-2\nu)]$, where E is the Young's modulus,[17] and ν is the Poisson ratio (taken as 0.3). Although the calculation of the bulk modulus often gives quite large errors, they do give reasonably good results in this case.

From plots of the density of states (Figs. 1–3), we can see that there is a low-lying band dominated by the s electrons which is separated from other bands by a narrow forbidden region (gap). This indicates that hybridization between the s band and other bands is not really important. There is a wider gap in the $D0_{22}$ structure and the hybridization due to the higher-lying energy bands is weakest in the $D0_{22}$ structure. This coincides with the results that the $D0_{22}$ structure has the highest total energy. The density-of-states values at the Fermi energy, $N(E_F)$, are 1.95, 4.60, and 3.77 states/eV f.u. for the $D0_{19}$, $D0_{22}$, and $L1_2$ structures. The $D0_{19}$ structure has the lowest value since the Fermi energy lies at a point very close to the bottom of a valley. By contrast, E_F lies

TABLE I. Calculated and experimental Wigner-Seitz radii (R_{WS}), heats of formation (ΔH), bulk moduli (B), and DOS at E_F [$N(E_F)$].

	LMTO			FLAPW			Experiment
	$D0_{19}$	$D0_{22}$	$L1_2$	$D0_{19}$	$D0_{22}$	$L1_2$	(for $D0_{19}$)
R_{WS} (a.u.)	2.98	2.98	2.98	2.94	2.94	2.94	2.99[5]
c/a				0.807	2.131		0.8007
ΔH (eV/atom)	0.29	0.27	0.29	0.28	0.25	0.27	0.26[14],0.29[15] 0.27[16](±0.01)
B (Mbar)	1.3	1.2	1.2	1.2	1.2	1.2	1.2
$N(E_F)$ (states/eV f.u.)	1.95	4.60	3.77	2.10	4.86	3.64	
$\Delta\epsilon$[a] (eV)	0.082	−0.24	0.17	0.095	−0.20	0.14	
Δn[b] (number of electrons)	0.12	−0.96	0.47				
$N(Z)^c_{min}$ (states/eV f.u.)	1.26	1.65	2.06				

[a] $\Delta\epsilon$ denotes the energy value of the minimum point relative to the Fermi energy in eV.

[b] Δn denotes the number of electrons which can be accommodated from the Fermi energy to the minimum point. Negative values mean that fewer electrons than that of Ti_3Al are needed for reaching the minimum point.

[c] $N(Z)_{min}$ is the density-of-states value at the minimum point.

at much higher values in both the $D0_{22}$ and the $L1_2$ structures. Such a correlation of stability with a low $N(E_F)$ has been emphasized by us before[8,10,12] and thus may again be used to explain why the $D0_{22}$ structure has the highest total energy and the $D0_{19}$ structure is more stable than the $L1_2$ structure although they have almost the same total energy.

By examining the structure of the density-of-states (DOS) curves, we can find one of the major minimum points near the Fermi energy for each of the three structures. The energy value at this minimum point relative to E_F, the number of electrons that can be accommodated from the Fermi energy to the minimum point, and density of states at the minimum point for the three structures are also listed in Table I. We see that the $L1_2$ structure would have the Fermi energy sitting at the minimum point if 0.47 more electrons were added to the unit cell—assuming the DOS curve to be unaffected by this change (in a rigid band shift). The DOS value for $L1_2$ at the minimum point is only 2.06 states/eV f.u., while the values for $D0_{19}$ and the $D0_{22}$ are 3.60 and 5.16 states/eV f.u., respectively, if we have 0.47 electrons added to the unit cell, as for the $L1_2$. By such a method, we might end up with a stable $L1_2$ phase.

By comparing the DOS curves with those calculated for pure Ti in its fcc (Ref. 18) and hcp (Fig. 4) structures and for the compound $TiAl_3$ (Ref. 8) in the same three structures, we find much more complex structure in the case of Ti_3Al. This large change in the DOS might be attributed to the combined effect of the substitutional Ti—Al bonds formed with the addition of Al and the strong Ti—Ti bonds. In pure Ti, there are strong Ti—Ti

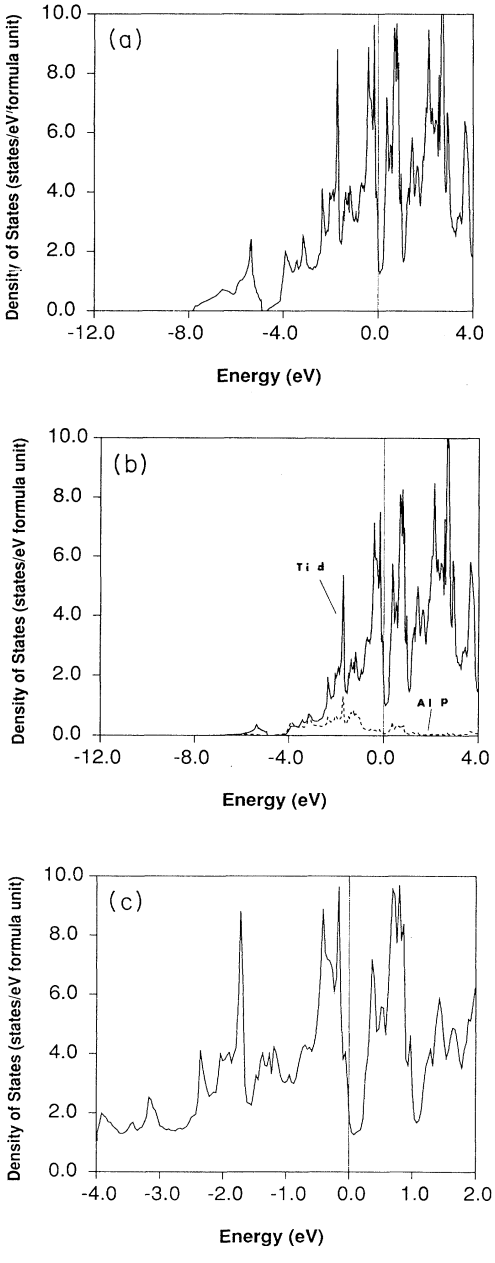

FIG. 1. (a) Calculated density of states for Ti_3Al ($D0_{19}$); (b) Ti d and Al p partial density of states calculated for Ti_3Al ($D0_{19}$); (c) calculated density of states for Ti_3Al ($D0_{19}$) enlarged around Fermi energy.

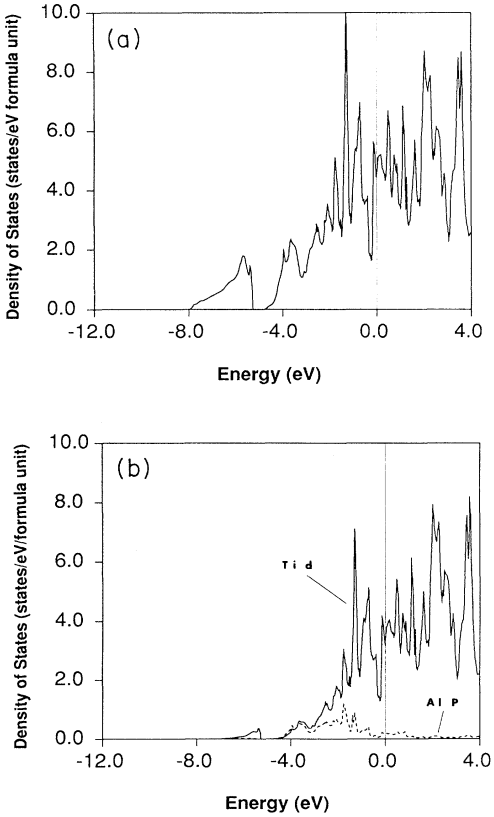

FIG. 2. (a) Calculated density of states for Ti_3Al ($D0_{22}$); (b) Ti d and Al p partial density of states calculated for Ti_3Al ($D0_{22}$).

bonds—and of course no Ti—Al ones. In $TiAl_3$, there are Ti—Al bonds, but not strong Ti—Ti ones. Both of their DOS curves have simpler structures. For pure Ti (hcp), only a small portion of s,p components and a tiny d tail extended to the region below -4.0 eV. As a result, the profile of the calculated density of states for[8] $TiAl_3$ is

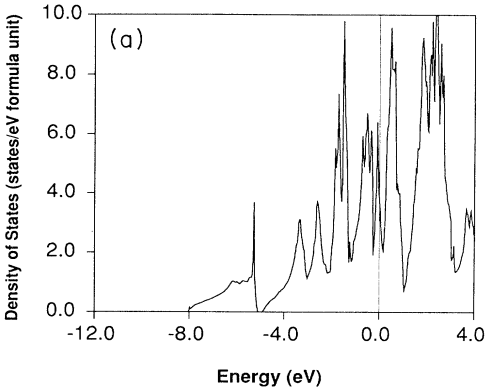

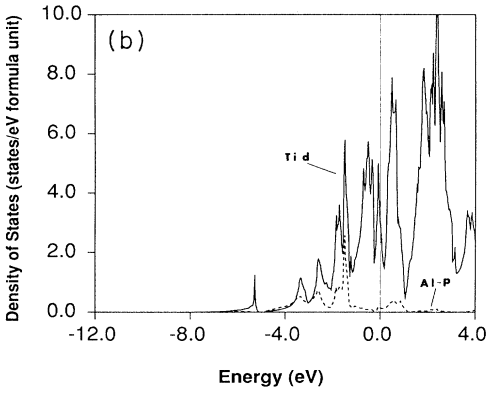

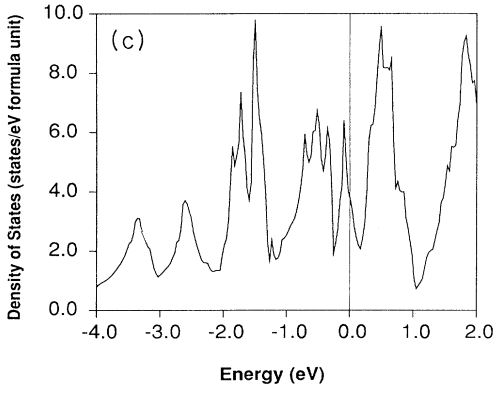

FIG. 3. (a) Calculated density of states for Ti_3Al ($L1_2$); (b) Ti d and Al p partial density of states calculated for Ti_3Al ($L1_2$); (c) calculated density of states for Ti_3Al ($L1_2$) shown on an enlarged scale around E_F.

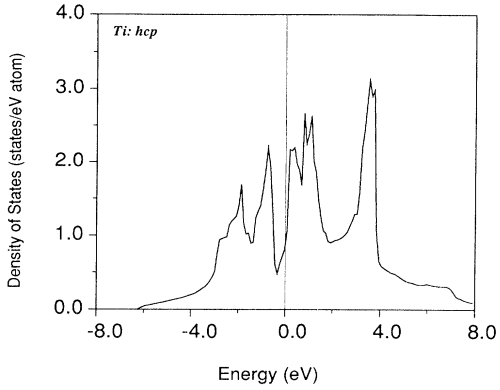

FIG. 4. Calculated density of states for pure Ti (hcp).

very much like that of the free-electron case (Al) in the region below -4.0 eV. For Ti_3Al, we found highly hybridized features in the same energy region which is mainly due to the interaction between Ti and Al atoms. In the region above -4.0 eV, the Ti d–Ti d interactions are dominant, as shown by a number of sharp peaks and valleys. One can still see some resemblance between the DOS results for pure Ti and Ti_3Al, although the relative strength and position are different for each case.

From band-character decompositions at the Γ point (Tables II–IV), we can see that strong hybridization between Ti d and Al p is still the main feature in $D0_{22}$, as in the $TiAl_3$ case. However, stronger hybridization between Ti d and Ti d makes $D0_{19}$ and $L1_2$ more stable. This is in contrast to the $TiAl_3$ case, where strong Ti d–Al p hybridization makes $D0_{22}$ the most stable one. As the distance between the Ti atoms in Ti_3Al is much closer than that in $TiAl_3$ ($\sim 70\%$ of the latter), this result is quite understandable. Comparing the electronic character of $D0_{19}$ and $L1_2$, we find that while the bonding is contributed almost totally by Ti d–Ti d hybridization in the $L1_2$ phase, Al p does play a role in contributing to the bonding in $D0_{19}$. Recalling that the calculated total energy is almost the same for $D0_{19}$ and $L1_2$, the stability problem is really a competition between Ti d–Ti d and the Al p–Ti d in Ti_3Al.

The relative strength of the bonding at the equilibrium volumes in our calculations can be obtained from the relative stability of the three structures. All three structures have the same nearest-neighbor configuration. The $D0_{22}$ unit cell has two Ti—Al bonds instead of a Ti—Ti and an Al—Al bond in the $D0_{19}$ and $L1_2$ structures as the second-nearest neighbors (of course, there are other second-nearest-neighbor bonds which are the same for the three structures). Since the total energy of the $D0_{22}$ structure is higher than that of the other two, and if we attribute this difference to different neighbor configurations up to second order, we can conclude that the two Ti—Al bonds are weaker than the sum of a Ti—

TABLE II. Band-character decomposition (in percent) of Ti_3Al ($D0_{19}$) at the Γ point by orbital angular momentum.

Energy		Al (in %)			Ti (in %)		
(eV)	Degeneracy	*s*	*p*	*d*	*s*	*p*	*d*
−7.65	1	42	0	0	57	1	0
−4.89	1	56	0	0	0	6	37
−2.37	1	0	24	0	0	1	75
−2.30	2	0	14	4	31	12	39
−2.07	1	5	0	2	9	10	74
−2.01	1	0	2	6	30	3	58
−1.81	1	0	38	1	10	36	14
−1.79	1	0	36	1	11	34	17
−1.31	2	0	2	7	1	2	89
−0.71	2	0	0	9	0	9	82
−0.25	1	0	32	0	0	7	61
0.01	1	4	0	3	4	50	39
0.04	1	0	22	0	0	64	14

Ti and an Al—Al bond. (Since Al is a good free-electron-type metal, the Al—Al bond would be expected to be much less important than the Ti—Ti bond.) Therefore, we come to the conclusion that the Ti-Ti bonding (more specifically, the dominant Ti *d* – Ti *d* bonding) plays a very important role when we consider the stability. The $D0_{19}$ and $L1_2$ structures have the same second-nearest-neighbor configuration. Now, when examining the third-nearest neighbors, the bond distance and number of the bonds are not at all the same. As the calculated total energy has the same value for the two structures, the difference in the third-nearest neighbors appears to be unimportant as far as the total energy is concerned. However, this difference changes the structure of the DOS and gives the different stability of the two structures.

It appears instructive to compare Ti_3Al with $TiAl_3$. In $TiAl_3$, the first-nearest neighbors include Ti—Al and Al—Al bonds, and Ti—Ti bonds only appear as second- and higher-order nearest neighbors. By contrast, in Ti_3Al, strong Ti—Ti bonds show up as the first-nearest neighbors. As discussed above, fewer strong second-nearest-neighbor Ti—Ti bonds in Ti_3Al make $D0_{22}$ the least favorable phase among the three structures. Thus, it is natural to speculate on the possible relation between the appearance of strong first-nearest-neighbor Ti—Ti bonds and the occurrence of enhanced second-nearest-neighbor Ti—Ti bonds in Ti_3Al.

B. FLAPW calculations

Using quadratic fittings, the equilibrium volume (in terms of Wigner-Seitz radius, R_{WS}) for the $D0_{19}$, $D0_{22}$, and $L1_2$ structures and the c/a ratio for the $D0_{19}$ and $D0_{22}$ structures were both determined from the calculations, as also shown in Table I. The calculated R_{WS} are 2.94 a.u. for all three structures, again showing consistency among the different phases. However, this value is about 2% smaller than experiment. This compares with a deviation of less than 0.5% from the LMTO calculations (cf. Table I) which is usually considered as a less precise approach. By comparing our results with other FLAPW calculations on aluminides,[11,19,20] the agreement of about 2% is not at all surprising, as our results are ob-

TABLE III. Band-character decomposition (in %) of Ti_3Al ($D0_{22}$) at the Γ point by orbital angular momentum.

Energy		Al (in %)			TiI[a] (in %)			TiII[a] (in %)		
(eV)	Degeneracy	*s*	*p*	*d*	*s*	*p*	*d*	*s*	*p*	*d*
−8.01	1	45	0	0	19	0	0	36	0	0
−2.59	1	5	0	6	0	0	26	14	0	48
−2.25	1	0	21	0	0	3	0	0	2	74
−1.54	1	0	8	4	0	3	15	0	0	70
−1.49	1	0	25	0	0	13	0	0	0	61
−1.47	1	0	18	2	0	10	5	0	0	66
−0.34	1	0	0	11	0	0	75	0	14	1
0.04	2	0	0	2	0	0	69	0	17	12

[a]TiI is the Ti atom on the (001) planes with equal amount of Ti atoms and Al atoms, where TiII is the Ti atom on the (001) planes with only Ti atoms [cf. Fig. 1(c)].

TABLE IV. Band-character decomposition (in %) of Ti_3Al ($L1_2$) at the Γ point by orbital angular momentum.

Energy (eV)	Degeneracy	Al (in %)			Ti (in %)		
		s	p	d	s	p	d
−7.72	1	43	0	0	55	0	2
−3.09	1	6	0	0	14	0	80
−1.66	2	0	0	12	12	0	76
−1.27	3	0	0	6	0	0	94
1.32	3	0	47	0	0	52	1

tained for 0 K, while the experiments are normally done at room temperature; further, the zero-point vibrational energy is left out in our calculations. The better agreement actually obtained from the LMTO calculations may be thought of as some cancellation of approximations made in the LMTO method to the above-mentioned effects on this particular case. The calculated c/a ratio for the $D0_{19}$ and $D0_{22}$ structures are 0.807 and 2.131, respectively, which are determined by the center of a group of ellipses which fit the calculated data points for each structure. The calculated value for the $D0_{19}$ structure is in very good agreement ($<1\%$) with the experimental value (0.8007). Recalling that the ideal c/a ratio for the $D0_{19}$ structure is 0.816, we see that our calculated value lies between the ideal and experimental values, showing that our theoretical approach is closer to the ideal case than are the experiments, which is also understandable. (Our calculations and the ideal case both refer to $T=0$ K, while experiments are normally done at much higher temperatures.) The value for the $D0_{22}$ structure deviates significantly less from the value 2.0 corresponding to the $L1_2$ than the observed value (2.234) for the $D0_{22}$ structure in $TiAl_3$. This may be the indication of the relatively lesser importance of the Ti—Al bonds in Ti_3Al than in $TiAl_3$, which is closely associated with the tetragonal distortion.

The formation energies for the $D0_{19}$, $D0_{22}$, and $L1_2$ structures are now 0.28, 0.25, and 0.27 eV/atom, respectively. These values are slightly smaller than those from the LMTO and are still in the range of experimental values (cf. Table I). Most importantly, the $D0_{19}$ is now energetically favorable—a result that the LMTO failed to produce. Although the difference between phases is small, they are distinguishable considering the high precision of the FLAPW method. Nevertheless, the energy difference is very small: this makes it feasible to stabilize the $L1_2$ phase by ternary alloy additions—as we argued from the LMTO results. The bulk moduli for all three phases are 1.2 Mbar, which is almost the same values as those obtained from the LMTO calculations and experiment. These results along with the results from an earlier $TiAl_3$ study[8] show that the bulk modulus of the titanium-aluminides determined from our *ab initio* approaches are quite reliable.

The density of states for the $D0_{19}$ and $L1_2$ structures are almost unchanged from the corresponding LMTO calculations except for some slight shift in relative position and height of the peaks and valleys. The density of states at the Fermi energy are 2.10, 4.86, and 3.64 states/eV f.u. for the $D0_{19}$, $D0_{22}$, and $L1_2$ structures, respectively, compared to 1.95, 4.60, and 3.77 states/eV f.u. from the LMTO calculations. Considering that the peaks and valleys are very steep near the Fermi energies of all three phases, the difference in values obtained by the two methods is rather small. For this reason, the density of states from the FLAPW calculations are not shown here. The Fermi energy is located near the bottom of the deepest valley on the downhill side for $D0_{19}$, near a group of peaks for $D0_{22}$, and in the middle between a modest peak and a modest valley for $L1_2$, just like those from the LMTO calculations. The energy bands (not shown here) from the two methods are almost the same for the low-lying parts. For the energies near the Fermi energy, the bands are shifted slightly (for several isolated portions) from one method to another. However, the main features are the same.

To further explore the bonding characters in order to investigate the possible $D0_{19}$ to $L1_2$ phase transition, the total valence-electron density and the valence-electron density at E_F for the (111) plane of the $L1_2$ and the (0001) plane of the $D0_{19}$ structures [Figs. 5(a), 5(b), 6(a), and 6(b), respectively] are plotted. By comparing the density for the two phases, we can see that the charge density is much more homogeneously distributed on the (111) plane of the $L1_2$ than on the (0001) plane of the $D0_{19}$ structure, on which two planes the atomic arrangements are virtually the same [the two planes are exactly the same if the c/a ratio for $D0_{19}$ is taken at the ideal value (0.816), cf. Figs. 1(a) and 1(b) of Ref. 8]. For the (111) plane of the $L1_2$ structure, there are only two kinds of interstitial positions: one is at the center of three adjacent atoms with a Ti atom sitting at the same place on the next (111) plane right above or below this one (denoted as position I hereafter), another is at the center of three adjacent atoms with an Al atom sitting at the same position on the next (111) plane right above or below this one (denoted as position II hereafter). Meanwhile, for the (0001) plane of the $D0_{19}$ structure, there are three kinds of interstitial positions: the first two are at the centers of three adjacent atoms with two Ti or Al atoms sitting at the same positions on the neighboring (0001) planes (denoted as positions I and II for those with two Ti and two Al atoms, respectively); the third one is at the center with nothing sitting at the same position on the neighboring (0001) planes (denoted as position III hereafter).

For the $L1_2$ phase, the charge density is quite flat at

position I and there is a small density valley in the middle position between the Ti and Al atoms, while a modest charge pileup is shown clearly at position II. Hence we come up with the argument that the bonding between Ti and Al is not prominent while that between Ti atoms becomes relatively important in this case. The valence-electron density at the Fermi energy (done with an energy window from the Fermi energy to 20 mRy below) supports such a statement since the direction of the strong pileup of these Ti electrons is towards position II which is the center of three Ti atoms on the same (111) plane, while the density is rather small along the line connecting Ti and Al atoms which is perpendicular to the direction mentioned above.

For the $D0_{19}$ structure, the charge around position III is at a local minimum because no atoms sit at the same position on the neighboring planes. Around positions I and II, the electron density is clearly higher than the corresponding positions in the $L1_2$ structure, as there are two Ti atoms or two Al atoms (positions I and II, respectively) at the same position on the neighboring planes, rather than one in the $L1_2$ case. The local pileup around position I is mainly due to the Ti atoms on the neighboring planes since the local environment for position I is

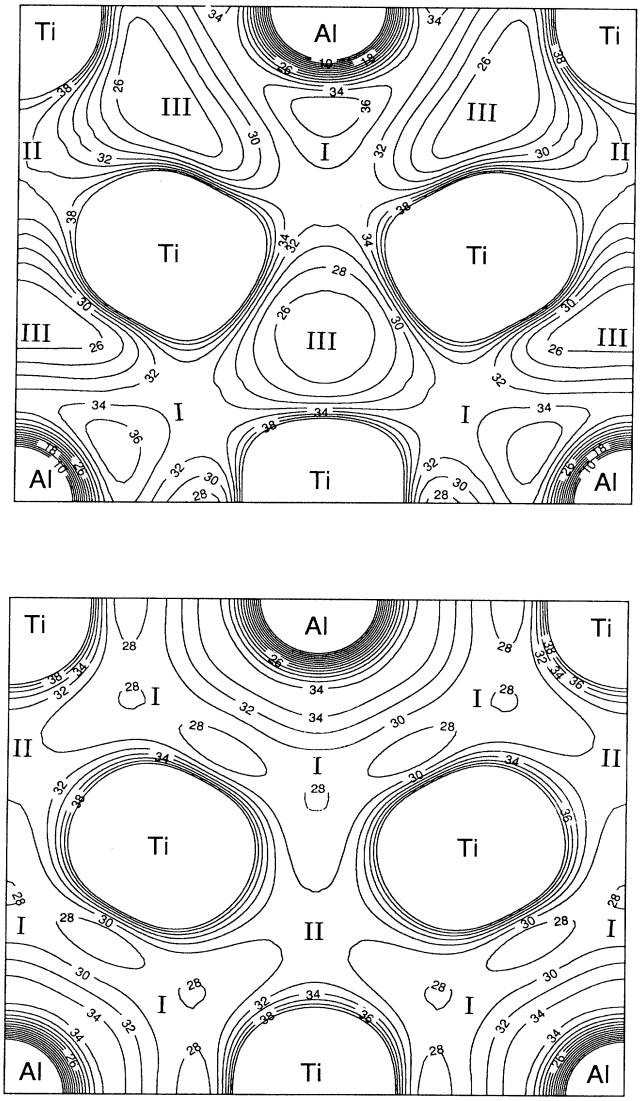

FIG. 5. (a) Total valence-electron density for Ti_3Al [(0001) plane in the $D0_{19}$]; (b) total valence-electron density for Ti_3Al [(111) plane in the $L1_2$]. The positions I, II, and III are discussed in the text.

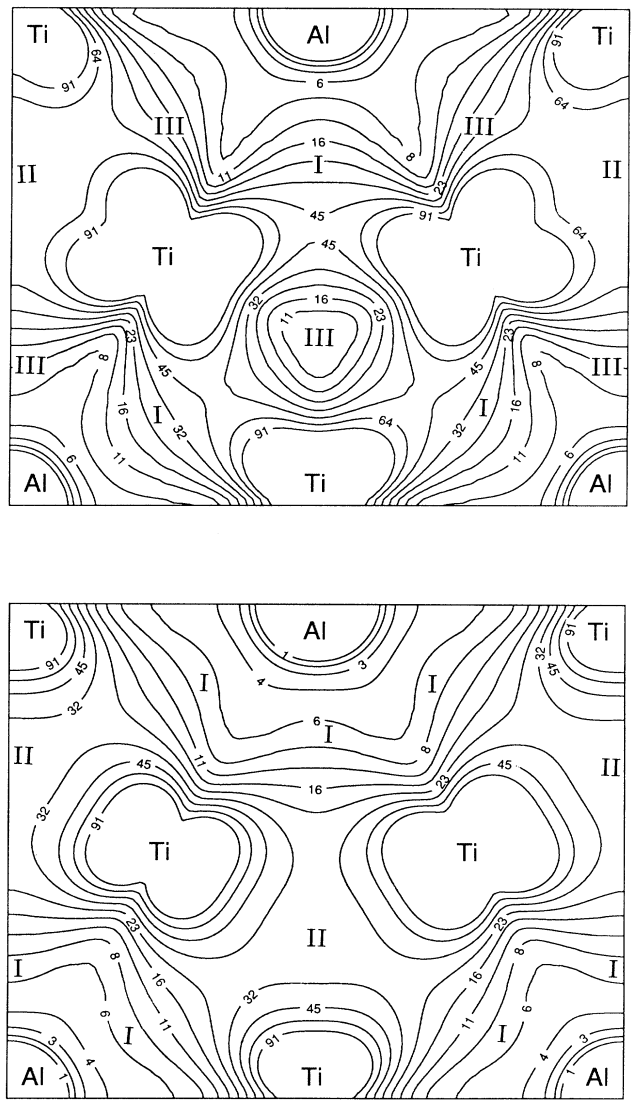

FIG. 6. Valence-electron density at the Fermi energy for Ti_3Al [(0001) plane in the $D0_{19}$]; (b) valence-electron density at the Fermi energy for Ti_3Al [(111) plane in the $L1_2$].

the same as one of the III positions except for the Ti atoms on the neighboring planes for position I. The high charge density around position II [surrounded by three Ti atoms on the same (0001) plane] indicates that the two Al atoms on the neighboring planes are the crucial factor because position II would be the same as one of the position III's if the two Al atoms on the neighboring planes are not taken into account.

Therefore, the direct bonding between the Ti and Al atoms is not strong at all, but the Al atoms do help form the Ti—Ti bond. The big difference in values of the valence-electron charge density tells us the directionality of the bondings in the $D0_{19}$ structure. This could be used in turn to explain the difficulty for providing enough slip systems in $D0_{19}$. The charge-density features seen around position II and position III (surrounded by three Ti atoms) in Fig. 6(a) further supported the argument above, there is strong Ti d bonding character around position II, while weak (if any) bonding around position III. These results agree with the generally accepted idea that a crystal with higher symmetry would provide more equivalent directions, therefore more capability for slip to occur.

IV. CONCLUSIONS

In conclusion, we have calculated the structural stability, cohesive properties, and electronic structure of Ti_3Al. The energy difference between the three structures is unexpectedly small with the $L1_2$ structure having almost the same total energy as the experimentally observed $D0_{19}$ structure. The calculated lattice constants are consistent among the different structures within either LMTO or FLAPW and agree well with experiment. Calculations of the formation energies and bulk moduli also give agreement with experiment to $<10\%$. The density-of-states value for the $D0_{19}$ structure is the lowest, and the stronger hybridization occurs in the $D0_{19}$ structure; both are indicative of its preferred stability relative to the other structures investigated. The charge-density plots illustrated interesting bonding features in the $D0_{19}$ and the $L1_2$ structures. The relatively homogeneous charge distribution in the $L1_2$ structure is an encouraging sign to improve the ductility by stabilizing the $L1_2$ structure with some third element addition.

ACKNOWLEDGMENTS

This work was supported by the U.S. Air Force Office of Scientific Research (Grant No. 88-03468) and by a grant of computer time at the Wright-Patterson Air Force Base Supercomputing Center. Discussions with D. Dimiduk are gratefully acknowledged.

*Present address: Department of Electrophysics, National Chiao-Tung University, 1001 Ta Hsueh Road, Hsinchu, Taiwan 30049.

†Present address: Department of Physics, University of Wisconsin–Milwaukee, P. O. Box 413, Milwaukee, WI 53201.

‡Present address: National Research Institute for Metals, 2-3-12 Nakameguro, Meguro-ku, Tokyo 153, Japan.

[1]J. C. Williams and M. J. Blackburn, in *Ordered Alloys,* edited by H. Kear, T. Sims, S. Stoloff, and J. H. Westbrook, (Claitor's, Baton Rouge, 1970), p. 425.

[2]S. M. Sastry and H. A. Lopsitt, Metall. Trans. **8A**, 1543 (1977).

[3]H. A. Lipsitt, D. Shechtman, and R. E. Schafrik, Metall. Trans. **11A**, 1369 (1980).

[4]M. Thomas, A. Vassel, and P. Veyssiere, Scr. Metall. **21**, 501 (1987).

[5]W. B. Pearson, *A Handbook of Lattice Spacings and Structures of Metals and Alloys* (Pergamon, New York, 1958).

[6]O. K. Anderson, Phys. Rev. B **12**, 3060 (1975).

[7]H. J. F. Jansen and A. J. Freeman, Phys. Rev. B **30**, 561 (1984).

[8]T. Hong, T. J. Watson-Yang, A. J. Freeman, T. Oguchi and J.-h. Xu, Phys. Rev. B **41**, 12462 (1990).

[9]B. I. Min, T. Oguchi, H. J. F. Jansen, and A. J. Freeman, J. Magn. Magn. Mater. **54-57**, 1091 (1986).

[10]J.-h. Xu, T. Oguchi, and A. J. Freeman, Phys. Rev. B **35**, 6940 (1987).

[11]X.-Q. Guo, R. Podloucky, and A. J. Freeman, Phys. Rev. B **40**, 2793 (1989).

[12]J.-h. Xu, T. Oguchi, and A. J. Freeman, Phys. Rev. B **36**, 4846 (1987).

[13]J.-h. Xu and A. J. Freeman, Phys. Rev. B **40**, 11927 (1989).

[14]O. Kubaschewski and W. A. Dench, Acta Metall. **3**, 339 (1955).

[15]*Smithells Metals Reference Book,* 6th ed., edited by E. A. Brandes (Butterworths, London, 1983).

[16]O. Kubashewski and G. Heymer, Trans. Faraday Soc. **56**, 473 (1960).

[17]S. N. Pastushenko, Fiz. Metal. Metalloved. **57**, 1035 (1984).

[18]*Calculated Electronic Properties of Metals,* edited by V. L. Moruzzi, J. F. Janak and A. R. Williams (Pergamon, New York, 1978).

[19]B. I. Min, A. J. Freeman, and H. J. F. Jansen, Phys. Rev. B **37**, 6757 (1988).

[20]X.-Q. Guo, R. Podloucky, and A. J. Freeman, Phys. Rev. B **42**, 10912 (1990).